Lack of *Il12rb2* signaling predisposes to spontaneous autoimmunity and malignancy

Irma Airoldi, Emma Di Carlo, Claudia Cocco, Carlo Sorrentino, Franco Fais, Michele Cilli, Tommaso D'Antuono, Mario Paulo Colombo, and Vito Pistoia

The interleukin-12 receptor β2 *(Il12rb2)* gene is silenced in tumor cells from different human B-cell malignancies as opposed to their normal counterparts. It was hypothesized that this silencing allows neoplastic B cells to escape the control exerted by IL-12 on their growth. The aim of this study was to investigate whether targeted inactivation of the *Il12rb2* gene in mice resulted into increased susceptibility to spontaneous tumor formation and immunopathology. *Il12rb2* gene–deficient animals developed in the first year of life immune-complex mesangial glomerulonephritis with serum antinuclear antibodies. In older animals, multiorgan lymphoid infiltrates with features of vasculitis and Sjögren syndrome were detected in association with systemic B- and T-cell activation. In half of aged animals, lymph node plasmacytoma or lung carcinoma was observed. A mechanism for spontaneous development of autoimmune pathology and B-cell tumors is suggested by a strong IL-6 up-regulation detected in splenocytes and lymphoid infiltrates associated with oligoclonal B-cell expansion. The emergence of lung tumors may likely be attributed to an interferon-γ (IFN-γ) deficiency secondary to lack of IL-12 signaling. The development of autoimmunity, lymphoproliferation, and B-cell tumors in *Il12rb2* knockout (KO) mice suggests that IL-12 functions physiologically to restrain aberrant B-cell activation. (Blood. 2005;106: 3846-3853)

Introduction

Interleukin-12 (IL-12) is a heterodimeric proinflammatory cytokine composed of 2 subunits, p35 and p40, that is produced predominantly by antigen-presenting cells (APCs).[1] IL-12 drives T helper 1 (Th1) responses, enhances T- and natural killer (NK)–cell cytotoxicity, and induces interferon-γ (IFN-γ) production by T and NK cells.[2-5] In addition, IL-12 exerts antitumor activity through IFN-γ–dependent and –independent mechanisms.[6-9]

The IL-12 receptor is a heterodimer composed of the β1 and β2 chains, both of which are needed for high-affinity binding of the cytokine and initiation of signal transduction.[10,11]

IL-12 belongs to a family of structurally related cytokines including IL-23 and IL-27. IL-23, which is formed by the IL-12p40 subunit and p19, binds to a receptor composed of IL-12Rβ1 and another chain, known as IL-23R.[12] Therefore, the IL-12p35 and the *Il12rb2* subunits are unique components of IL-12 and IL-12R, respectively.[12]

Recently, we[13] have shown that IL-12 contributed to the regulation of normal human B-cell function through stimulation of immunoglobulin M (IgM) synthesis and IFN-γ production. Furthermore, we[14] have shown that, at variance with their normal counterparts, neoplastic B cells from various chronic lymphoproliferative disorders did not express the *Il12rb2* gene due to methylation of a cytosine plus guanine (CpG) repeated island within exon 1.[14] Silencing of this gene resulted in enhanced tumor-cell survival and proliferation in vitro. Finally, human recombinant IL-12 strongly reduced the tumorigenicity of *Il12rb2*–transfected Burkitt lymphoma cells in severe combined immunodeficient/nonobese diabetic (SCID/NOD) mice through antiproliferative and proapoptotic effects coupled with angiogenesis inhibition.[14] These findings led us to conclude that the *Il12rb2* gene acts as a tumor suppressor in human chronic B-cell malignancies and to hypothesize that the IL-12/IL-12R system may be involved in the control of aberrant B-cell proliferation and expansion.

We have now tested this hypothesis in *Il12rb2* genetically deficient (*Il12rb2* knock-out [KO]) mice maintained in specific pathogen-free conditions and followed these mice throughout their life span. These animals developed spontaneously immune-complex glomerulonephritis and ectopic oligoclonal B-cell infiltrates. Furthermore, half of aged mice developed plasmacytoma and lung epithelial tumors.

Materials and methods

Mice

Il12rb2 gene–targeted C57BL/6J (KO) mice were purchased from the Jackson Laboratory (Bar Harbor, ME) and housed in sterile enclosures

From the Laboratory of Oncology, G. Gaslini Institute, Genova, Italy; the Department of Oncology and Neurosciences, and Center of Excellence on Aging (CeSI), G. D'Annunzio University, Chieti, Italy; the Human Anatomy Section, Department of Experimental Medicine, University of Genova, Genova, Italy; the Animal Model Facility, Istituto Nazionale per la Ricerca sul Cancro, Genova, Italy; and the Immunotherapy and Gene Therapy Unit, Department of Experimental Oncology, Istituto per lo Studio e la Cura dei Tumori, Milan, Italy.

Submitted May 23, 2005; accepted July 28, 2005. Prepublished online as *Blood* First Edition Paper, August 4, 2005; DOI 10.1182/blood-2005-05-2034.

Supported by grants from L'Associazione Italiana per la Ricerca sul Cancro (AIRC), Milan, Italy, to V.P. and M.P.C.; and Fondazione Cassa di Risparmio Provincia di Chieti to E.D.C. I.A. is supported by Fondazione Gaslini, Genoa, Italy. C.C. is the recipient of a fellowship from Fondazione Italiana per la Ricerca sul Cancro (FIRC), Milan, Italy.

I.A. and E.D.C. contributed equally to this work.

An Inside *Blood* analysis of this article appears at the front of the issue.

Reprints: Irma Airoldi, Laboratory of Oncology, G. Gaslini Institute, Largo G. Gaslini 5, 16148 Genova, Italy; e-mail: laboncologia@ospedale-gaslini.ge.it.

The publication costs of this article were defrayed in part by page charge payment. Therefore, and solely to indicate this fact, this article is hereby marked "advertisement" in accordance with 18 U.S.C. section 1734.

under specific pathogen-free conditions up to 26 months. Age-matched C57BL/6J wild-type (WT) mice (Harlan Italy, San Pietro al Natisone, Italy) were used as controls throughout. All procedures involving animals were performed with respect to the national current regulations (D.L. 27/01/1992, n. 116) regarding the protection of animals used for scientific purposes, and research protocols were reviewed and approved by the Institutional Animal Care and Use Committee (IACUC).

Every other month, 3 to 6 KO and 3 WT mice were killed in a CO_2-saturated chamber and autopsies were carried out. At the same time points, peripheral blood was collected from the retro-orbital sinus and centrifuged at 500*g* for 10 minutes at 4°C. Serum was isolated and stored at −20°C. In some experiments, blood was drawn in EDTA (ethylenediaminetetraacetic acid) and used for hemoglobin and hematocrit assessment, as well as for red blood cells, white blood cells (WBCs), differential WBCs, and platelet counts. For cryoglobulin search, blood was collected using a prewarmed syringe and incubated for 2 hours at 37°C before being centrifuged at 500*g* for 10 minutes. Serum was then stored for 3 days at +4°C and inspected for the presence of cryoglobulins. Urines were collected and stored at −20°C. Spleen, lymph nodes, stomach, gut, kidney, liver, salivary glands, and lungs were routinely processed for histologic evaluation or immunohistochemistry. Cell suspensions obtained from these organs were frozen in liquid nitrogen and subsequently used for flow cytometry studies and nucleic acid extraction. Soon after birth, the genotype of each mouse was determined by polymerase chain reaction (PCR) analysis of genomic DNA extracted from tail using *Il12rb2*–specific primers.[15]

Antinuclear and anti-DNA antibody assays

Serum from age-matched KO and WT mice was tested for the presence of antinuclear and anti-DNA antibodies, using slides coated with Hep-2 cells or with Crithidia luciliae (Kallestad; Sanofi Diagnostics Pasteur, Chaska, MN), respectively, according to standard methods. Briefly, slides were incubated for 30 minutes at room temperature with various dilutions of serum in phosphate-buffered saline (PBS). After 5 washings with PBS, slides were incubated with fluorescein isothiocyanate (FITC)–conjugated rabbit anti–mouse Ig (DAKO, Glostrup, Denmark) for 30 minutes at room temperature. After further washing, slides were stained for 1 minute with Evans Blue diluted in PBS and visualized under a fluorescence microscope (Nikon E1000; Nikon Instruments, Tokyo, Japan), using a Zeiss PLAN-NEOFLUAR 100 ×/1.30 numeric aperture (NA) oil objective with a 10 × eyepiece. Images were captured using a Nikon Coolpix 990 and processed using Microsoft PhotoDraw version 1.0 (Microsoft, Redmond, WA).

Antibodies, reagents, and flow cytometry

Intracellular and surface staining were performed as previously described.[16] All of the following antibodies, as well as isotype-matched control antibodies, were purchased from Pharmingen (San Diego, CA): FITC- and phycoerythrin (PE)–conjugated CD11c, FITC- and PE-conjugated CD11b, FITC- and PE-conjugated CD19, FITC- and PE-conjugated CD69, Cychrome–conjugated CD3, FITC- and PE-conjugated CD4, FITC-conjugated CD8, PE-conjugated anti-NK1.1, PE-conjugated anti–IL-4, PE-conjugated anti–IL-6, FITC-conjugated anti–IL-10, FITC-conjugated anti–IFN-γ, tricolor (TC)–conjugated B220, rat anti–mouse IL-12, and FITC-conjugated goat anti–rat Ig.

Cell suspensions from spleen, kidney, and liver were cultured for 16 hours in RPMI 1640 medium (Seromed-BiochromKG, Berlin, Germany) supplemented with 10% FCS (Seromed) in the absence of stimuli. Brefeldin A (2.5 μg/mL; Sigma-Aldrich, Saint Louis, MO) was added to the cultures to allow intracellular accumulation of produced cytokines. Cells were subsequently permeabilized and tested for intracellular expression of IL-6, IL-4, IFN-γ, and IL-10 by flow cytometry.[13]

In some experiments, splenocyte-cell suspensions were enriched for monocytes by adherence to plastic for 1 hour at 37°C in 5% CO_2. Nonadherent cells were transferred into a new flask and cultured for 36 hours in the presence of lipopolysaccharide (LPS, 1 μg/mL; Sigma-Aldrich), CpG (250 μg/mL; TIB Molbiol, Genova, Italy),[17] calcium ionophore (250 ng/mL; Sigma-Aldrich), and phorbol myristate acetate (PMA, 10 ng/mL; Sigma-Aldrich), phytohemagglutinin (PHA, 200 ng/mL; Sigma-Aldrich), with or without murine recombinant IL-12 (rIL-12, 5-70 ng/mL; R&D Systems, Minneapolis, MN).

Adherent cells were cultured for 36 hours in the presence of LPS (1 μg/mL; Sigma-Aldrich), CpG (250 μg/mL; TIB Molbiol), calcium ionophore (250 ng/mL, Sigma-Aldrich), and PMA (10 ng/mL; Sigma-Aldrich), with or without murine rIL-6 (100 ng/mL; ImmunoTools, Friesoythe, Germany). Thereafter, brefeldin A (2.5 μg/mL; Sigma-Aldrich) was added to the cultures and cells were detached from plastic using a scraper.

Intracellular expression of IL-6 and IL-12 was assessed by flow cytometry.

Cells were scored using a FACScan analyzer (Becton Dickinson, San Jose, CA), and data were processed using CellQuest software (Becton Dickinson). The threshold line was based on the maximum staining obtained with irrelevant isotype-matched monoclonal antibody (mAb), used at the same concentration as test mAb. Negative cells were defined such that less than 1% of cells stained positive with control mAbs. Cells labeled with test antibody that were brighter than those stained with isotypic control antibody were defined as positive.

Histology and immunohistochemistry

For histologic evaluation, tissue samples were fixed in 10% neutral buffered formalin, embedded in paraffin, sectioned at 4 μm, and stained with hematoxylin-eosin (H&E) and, when required, with periodic acid-Shiff (PAS), Congo red, and trichrome stains.

For immunohistochemistry, formalin-fixed, paraffin-embedded, or acetone-fixed cryostat sections were immunostained with anti-B220 (CD45R; clone RA3-6B2), anti-CD43 (Ly-48, Leukosialin; clone S7), anti-IgG1 (clone A85-1), anti–IL-6 (clone MP5-20F3), anti–IL-4 (clone 11B11), anti–IL-10 (clone JES5-16E3), anti–IFN-γ (clone XMG1.2), anti–peripheral lymph node addressin (PNAd) (clone MECA-79), and anti-CD138 (clone 281-2) (all from Pharmingen); anti–follicular dendritic cells (FDCs; clone FDC-M2) (Immunokontact, Abingdon, United Kingdom); anti–complement C3 and anti-IgG (both from Cappel, Aurora, OH); anti-CD3 and anti–proliferating cell nuclear antigen (PCNA) (clone PC10) (both from DAKO); anti-CD69 (H1.2F3) (Santa Cruz Biotechnology, Santa Cruz, CA); anti-CD56 (N-CAM; clone NCAM-OB11) (Sigma-Aldrich, St Louis, MO); and anti–mouse κ or λ Ig chains (both from Southern Biotechnology, Birmingham, AL). After washing, sections were overlaid with biotinylated rabbit antirat or goat antirabbit, or with horse anti–mouse or horse anti–goat Ig (Vector Laboratories, Burlingame, CA) for 30 minutes. Unbound Ig was removed by washing, and slides were incubated with avidin-biotin complex (ABC)/alkaline phosphatase (DAKO).

Double immunofluorescent staining of frozen tissue sections

Acetone-fixed frozen sections were washed for 5 minutes in PBS and incubated for 30 minutes with primary Ab. Slides were then washed in PBS for 5 minutes. Next, sections were incubated for 30 minutes with biotinylated secondary Ab, washed, and incubated with Alexa Fluor 488–conjugated StreptAvidin (Molecular Probes, Eugene, OR) for 20 to 30 minutes. After washing, sections were incubated for 30 minutes with the second primary Ab, washed again, and incubated for 30 minutes with biotinylated secondary Ab. After further washing, sections were incubated with Alexa Fluor 594–conjugated StreptAvidin (Molecular Probes) for 20 to 30 minutes and then washed. Cross-reaction between the first secondary Ab and Alexa Fluor 594 was prevented by saturation of its binding sites with Alexa Fluor 488. Slides were mounted with Vectashield medium (Vector Laboratories) and examined with a Zeiss LSM 510 Meta laser scanning confocal microscope (Zeiss, Oberkochen, Germany). Objectives used include Leica C PLAN 100 ×/1.25 NA oil (Figure 1A,B,E,F); C PLAN 63 ×/0.75 NA (Figures 1G-H, 5A-G); and N PLAN 40 ×/0.65 NA (Figures 2B, 3A-C, 5H). All images were captured with a 10 × eyepiece. Images were captured and processed as described in "Antinuclear and anti-DNA antibody assays."

Ig gene rearrangement studies by Ig complementarity determining region 3 (CDR3) spectratyping

DNA was extracted from spleen-, kidney-, and liver-cell suspensions using the GenElute mammalian genomic DNA miniprep kit from Sigma-Aldrich, according to the instructions of the manufacturer.

DNA (100 ng) was amplified using 200 μM deoxynucleoside triphosphates (dNTPs), 1.5 mM $MgCl_2$, and 1.25 U Platinum Taq (Invitrogen, Carlsbad, CA) in a final volume of 20 μL. The following fast performance liquid chromatography (FPLC) purified primers (Invitrogen) were used for amplification: mu1 forward (FW), CAG CTC AGC AGC CTG ACA TCT; mu2 FW, GAG CTC CAC AGC CTG ACA TCT; mu3 FW, GAG CTT AGT AGA TTG ACA TCT; and muJH reverse (RV), CTY ACC TGA GGA GAC KGT GA. MJH RV primer was labeled at 5′ with 6-carboxy-fluorescein (FAM) fluorophore. Forward primer design was based on immunoglobulin heavy chain (IgV_H) chain sequence available on the ImMunoGeneTics (IMGT) database[30] and took advantage of common sequences existing in the framework 3 (FR3) region of about 55% of IgV_H regions. Forward primers were admixed and used in conjunction with the MJH (reverse) primer at a final concentration of 400 nM each. Cycling reaction was as follows: 30 seconds at 94°C, 10 seconds at 54°C, and 5 seconds at 72°C for 35 cycles. The reaction was amplified in a Mastercycler Personal (Eppendorf, Hamburg, Germany). PCR products were incubated with 0.5 U T4 DNA polymerase (Invitrogen) for 30 minutes at 37°C to remove nontemplate nucleotide additions and purified using Montage PCR columns (Millipore, Billerica, MA). PCR products were denatured in 15 μL formamide (Applied Biosystems, Monza, Italy) at 94°C for 5 minutes and transferred on ice. Products were run on an automated sequenator (310 Genetic Analyzer; Applied Biosystems) and analyzed with Genescan software (Applied Biosystems).

Results

Development of immune-complex–mediated glomerulonephritis in *Il12rb2* KO mice

Il12rb2 KO C57BL/6J mice maintained under specific pathogen-free conditions were monitored from the age of 2 to 26 months for spontaneous development of immune-mediated diseases or tumors in comparison with WT mice of the same genetic background. The life span of *Il12rb2* KO mice did not differ from that of their WT counterparts, and palpable masses, abdominal distension, weight loss more than 10%, or ruffled fur was never observed in either group.

Kidney histologic examination disclosed mesangio-proliferative glomerulonephritis in 21 of 26 mice that first manifested at the age of 3 months and progressed with aging. Three of the unaffected mice were killed when 2 months old, while the remaining negative 2 were 8 months old. Lesions consisted of mesangial-cell proliferation and mesangial-matrix increase with secondary glomerular enlargement (Figure 1B). These abnormalities, which were not detected in age-matched WT mice (Figure 1A), were focal and did not extend to the entire glomerulus.

Immunohistochemical staining revealed mesangial deposition of IgG (Figure 1C) and of the C3 complement component in 16 (76%) of 21 *Il12rb2* KO mice (Figure 1D), indicating an immune-complex–mediated glomerulonephritis.

Progression of mesangio-proliferative glomerulonephritis to a sclerosing pattern was occasionally observed (Figure 1E-F). In elderly *Il12rb2* KO mice, glomeruli showed lympho-plasmacytoid infiltrates (Figure 1G-H).

Blood chemistry showed normal hemoglobin and hematocrit values, as well as normal erythrocyte, platelet, total, and differential WBC counts in 12 *Il12rb2* KO mice tested at different ages. Cryoglobulin search yielded negative results. No proteinuria was detected in 24 mice tested at different ages. In this respect, human mesangial proliferative glomerulonephritis is characterized by occasional detection of low-level proteinuria.

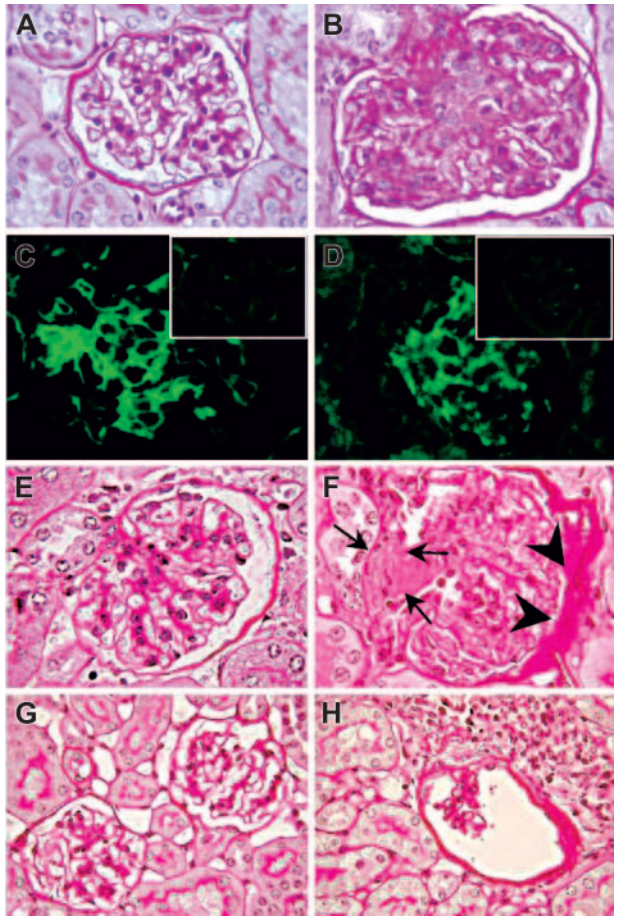

Figure 1. Mesangioproliferative glomerulonephritis in *Il12rb2* KO mice. A glomerulus from an 8-month-old WT mouse displays the tuft of capillaries with an open lumen filled by erythrocytes and supported by a delicate branching framework of mesangium (A, PAS staining). In contrast, a glomerulus from an age-matched *Il12rb2* KO mouse shows mesangial enlargement caused by mesangial hypercellularity (blue-stained nucleus) and matrix increase (fuchsia-stained material) resulting in capillary compression and occlusion (B, PAS staining). Immunofluorescent staining shows diffuse mesangial immunoreactivity for IgG (C) and for C3 (D) along the glomerular capillary loops in an *Il12rb2* KO mouse, as opposed to the negative staining of glomeruli from an age-matched WT mouse (insets in C and D, respectively). H&E staining of kidney sections from a 21-month-old *Il12rb2* KO mouse revealed, in contrast with the normal glomerulus from an aged-matched WT mouse (E), an advanced sclerosing glomerulonephritis with crescent formation (arrows) and adhesion to Bowman capsule, associated with thickening of its parietal layer (F). Altered glomeruli compressed by lympho-plasmacytoid infiltrates are observed in a 26-month-old *Il12rb2* KO mouse (H), but not in an age-matched WT mouse (G). Magnification: (A-F) × 1000; (G-H) × 630.

Serum antinuclear antibodies were found at a titer ranging from 1:80 to 1:160 in 12 (92%) of 13 *Il12rb2* KO mice with histologically proven glomerulonephritis, but not in WT mice (0/15). Anti-DNA antibodies were absent from serum of both *Il12rb2* KO and WT mice.

Functional alterations in the spleen from *Il12rb2* KO mice

We next investigated whether *Il12rb2* KO mice presented abnormalities of secondary lymphoid organs.

Until the age of 8 to 12 months, morphologic changes in the spleen and lymph nodes were detected in *Il12rb2* KO or WT mice. Accordingly, flow cytometric analysis of spleen-cell suspensions

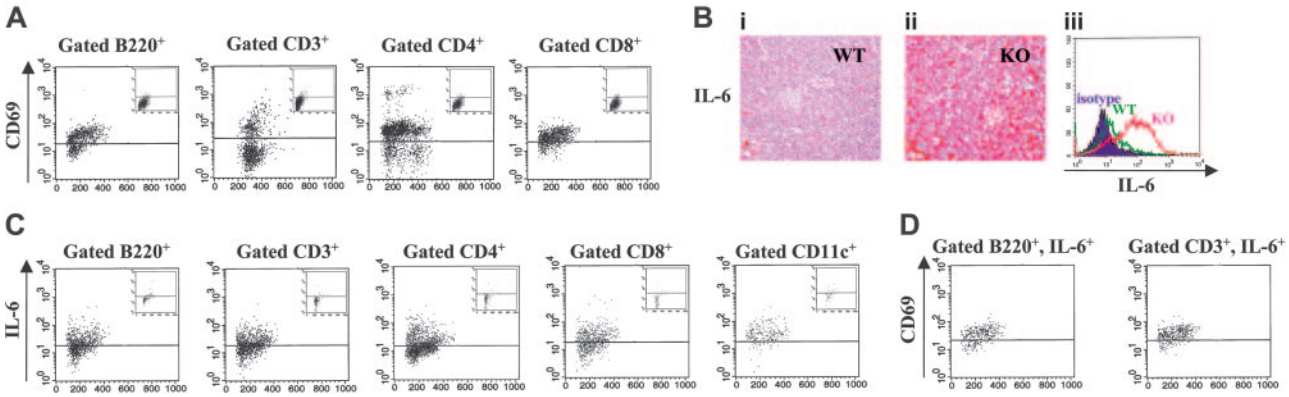

Figure 2. IL-6 overexpression and immune activation in the spleen of *Il12rb2* KO mice older than 12 months. (A) Expression of the CD69 activation marker on splenocytes from an 18-month-old *Il12rb2* KO mouse and an age-matched WT mouse (insets). Cells were stained with CD69 mAb in combination with anti-B220, CD3, CD4, or CD8 mAb and gated on the latter markers. Dot-plots are shown. (Bi-ii) Immunohistochemical staining of spleen tissue sections from an 18-month-old WT mouse (Bi) and an age-matched *Il12rb2* KO mouse (Bii) with anti–IL-6 mAb (magnification, × 400). (Biii) Flow cytometric analysis of intracellular IL-6 in splenocytes from an 18-month-old *Il12rb2* KO mouse (KO, right profile) and an age-matched WT mouse (WT, middle profile). Isotypic control staining (isotype), shown in the left profile, was superimposable for both animals. Cells were cultured without stimuli for 16 hours in the presence of brefeldin A to allow intracellular accumulation of synthesized IL-6, permeabilized, and analyzed. (C) Intracellular expression of IL-6 was investigated by flow cytometry following double staining of splenocytes from an 18-month-old *Il12rb2* KO mouse and an age-matched WT mouse (insets) with anti-B220, CD3, CD4, CD8, or CD11c, and anti–IL-6 mAbs. Cells were cultured as indicated in panel B, permeabilized, and analyzed setting the gate on $B220^+$, $CD3^+$, $CD4^+$, $CD8^+$, or $CD11c^+$ splenocytes. Dot-plots are shown. (D) Tricolor staining of splenocytes from an 18-month-old *Il12rb2* KO mouse with B220 or CD3 mAbs in combination with CD69 and anti–IL-6 mAbs. Gate was set on $B220^+$, $IL\text{-}6^+$ or $CD3^+$, $IL\text{-}6^+$ cells. Dot-plots are shown.

showed similar proportions of $CD3^+$, $CD4^+$, and $CD8^+$ T cells, $CD19^+$ B cells, $NK1.1^+$ NK cells, $CD11b^+$ macrophages, and $CD11c^+$ myeloid dendritic cells in both groups of mice.

Starting from the age of 13 months, development of secondary lymphoid follicles and $CD138^+$ plasma-cell hyperplasia was observed in the spleen and lymph nodes from *Il12rb2* KO mice, in association with spleen white pulp expansion (not shown). These morphologic features suggested an ongoing process of immune activation. As shown in Figure 2A, the large majority of B cells and T cells, either $CD4^+$ or $CD8^+$, expressed the CD69 early activation antigen, confirming a generalized splenocyte activation.

Constitutive IL-6 expression was detected by immunohistochemistry in the spleen of 13- to 26-month-old *Il12rb2* KO mice but not in age-matched WT mice (Figure 2Bi and 2Bii, respectively). In contrast, constitutive production of IFN-γ, IL-4, and IL-10 was barely detectable in both *Il12rb2* KO and WT mice at any age tested, as assessed by immunohistochemistry and flow cytometry (not shown).

To investigate the cellular source of IL-6, splenocyte suspensions from *Il12rb2* KO and WT mice older than 13 months were double stained for surface CD3, CD4, CD8, B220, or CD11c and intracellular IL-6. As shown in the representative experiment of Figure 2C, gated $B220^+$ B cells, $CD3^+$ T lymphocytes (both $CD4^+$ and $CD8^+$), and $CD11c^+$ myeloid dendritic cells produced IL-6. Figure 2C also shows very low IL-6 production in the same splenocyte subsets from a representative age-matched WT mouse (insets). These results were confirmed by double immunofluorescence staining of frozen spleen tissue sections (not shown).

In order to investigate the relationships between immune activation and IL-6 production, splenocytes from *Il12rb2* KO mice were triple stained with anti-B220 or CD3 mAbs, in combination with mAbs to IL-6 and CD69. Flow cytometric analysis demonstrated that the large majority of gated $B220^+$, $IL\text{-}6^+$ B cells and $CD3^+$, $IL\text{-}6^+$ T cells expressed the CD69 activation marker (Figure 2D).

Development of a multiorgan lymphoproliferative disorder in *Il12rb2* KO mice

Starting at the age of 12 months, infiltrates involving the kidney, the liver, and the major salivary glands manifested as diffuse lymphocyte bundles (Figure 3Ai) in 54% (14/26) of *Il12rb2* KO mice but not in WT mice. These infiltrates had a periarteriolar distribution featuring systemic vasculitis.

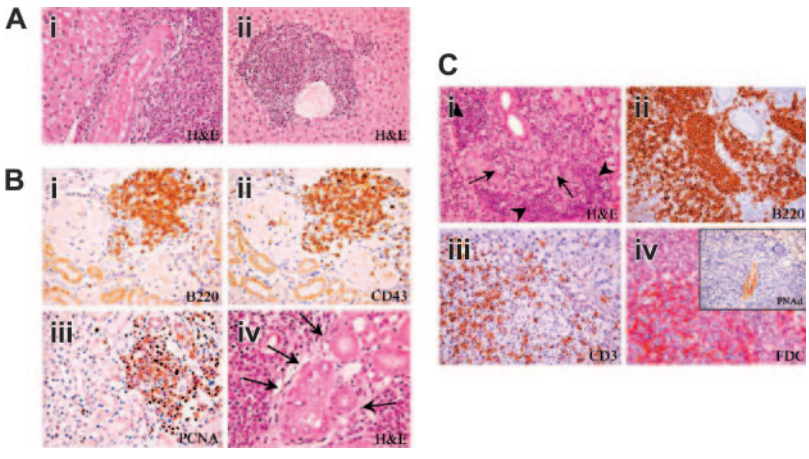

Figure 3. Development of multiorgan lymphoid infiltrates in *Il12rb2* KO mice. (A) Liver from a 15-month-old *Il12rb2* KO mouse shows periarteriolar lymphoid cuff (Ai). At the age of 18 months, the ectopic lymphoid infiltrate appears arranged in follicle-like structures (Aii). Magnification, × 400; H&E staining. (B) Ectopic lymphoid infiltrates in the kidney from a 18-month-old mouse (Bi-iv). These infiltrates are mostly composed of $B220^+$ (Bi), $CD43^+$ (Bii), and $PCNA^+$ (Biii) cells and compress the glomeruli and tubules. Lymphoid aggregates can invade epithelial structures (lymphoepithelial lesions indicated by arrows in Biv). Magnification, × 400. (C) Lymphocytic infiltration develops in the submandibular gland of a 15-month-old mouse (Ci). The centroblastic-centrocytic follicular infiltrate (Ci, arrows) is predominantly composed of $B220^+$ B cells (Cii), bordered by small mature lymphoid cells (Ci, arrowheads) displaying a $CD3^+$ T-cell phenotype (Ciii), with intermingled $FDC\text{-}M2^+$ cells (Civ). This ectopic lymphoid infiltrate organizes close to $PNAd^+$ vessels (inset in Civ). Magnification, × 400.

Table 1. Pathologic features of aged *Il12rb2* KO mice

Age, mo; n = 13	Immune-complex glomerulonephritis	Multiorgan lymphoid infiltrates			Tumors	
		Kidney	Liver	Salivary glands	Lymph-node plasmacytoma	Lung carcinoma
15	+	+	+	+	+	Not tested
15	+	+	+	−	−	Not tested
16	+	+	+	+	−	Not tested
16	+	+	+	−	−	Not tested
17	+	+	+	−	−	−
18	+	+	+	−	+	−
18	+	+	+	+	−	+
21	+	+	+	+	+	−
21	+	+	+	−	+	−
22	+	+	+	−	−	+
24	+	+	+	−	−	−
24	+	+	+	+	−	−
26	+	+	+	−	−	Not tested
Affected mice, %	13/13 = 100	13/13 = 100	13/13 = 100	5/13 = 40	4/13 = 31	2/8 = 25

Infiltrates organized into lymphoid follicle-like structures were detected in the liver (Figure 3Aii) and the kidney (Figure 3B) from all mice older than 15 months (Table 1). Similar infiltrates were observed in the parotid and submaxillary glands from 5 of 13 *Il12rb2* KO mice (Table 1; Figure 3Ci), where occasional lympho-epithelial lesions, characterized by close interactions among epithelial, T, and B cells, were detected (Figure 3Biv).

Follicle-like structures contained predominantly $B220^+$ B cells (Figure 3Bi,Cii), bordered by small $CD3^+$ T lymphocytes (Figure 3Ciii) and sparse plasma cells, with intermingled FDC-$M2^+$ cells (Figure 3Civ). Most lymphocytes clustered close to $PNAd^+$ high endothelial venules (Figure 3Civ, inset) and expressed the PCNA proliferation antigen (Figure 3Biii) as well as CD43, a pro/pre–B-cell and plasma-cell marker that is up-regulated in chronically activated ectopic B cells[18] (Figure 3Bii). The histopathologic findings in the salivary glands of *Il12rb2* KO mice were similar to those of the Sjögren syndrome.

Immunophenotyping by flow cytometry of the organized lymphoid infiltrates in the kidney and the liver showed that they were composed of $CD19^+$, $B220^+$ B lymphocytes (53%-62% for kidney and 70%-84% for liver, n = 5) and $CD3^+$ T cells (38%-47% for kidney and 16%-30% for liver, n = 5). T cells were either $CD4^+$ or $CD8^+$ (45%-55% for both cell fractions in the kidney; 54%-56% $CD4^+$ and 44%-46% $CD8^+$ cells in the liver). Rare $CD138^+$ plasma cells were detected.

By intracellular staining, 6% to 17% of the liver lymphocytes from *Il12rb2* KO mice (n = 10) were found to produce IL-6 in the absence of stimuli (Figure 4Ai). In contrast, IL-6 was not detected in liver lymphocytes from age-matched WT mice. The IL-6–producing liver lymphocytes from *Il12rb2* KO mice were $B220^+$ B cells (63%-76%, n = 5) (Figure 4Aii) and $CD3^+$ T cells (24%-47%, n = 5). Both $CD4^+$ and $CD8^+$ T cells produced IL-6, as shown in the representative experiment of Figure 4A (iii and iv, respectively).

Of the kidney lymphocytes, 5% to 11% produced IL-6; of these, 59% to 71% were $B220^+$, $CD19^+$ B cells (n = 5) and 29% to 41% were $CD3^+$ T cells (n = 5).

In order to analyze the clonality of expanded B cells, Ig gene rearrangement studies with kidney-, liver-, and spleen-cell suspensions from 6 of 14 *Il12rb2* KO mice were performed. Kidney and liver infiltrating B cells displayed an oligoclonal repertoire, as opposed to the polyclonal one detected in spleen B cells from the same animals (Figure 4B). Spleen, liver, and kidney B cells from the 4 control mice showed a polyclonal repertoire (Figure 4B, and data not shown).

Detection of lymph node plasmacytoma and epithelial lung tumors in *Il12rb2* KO mice

Lymph nodes from 4 of 13 mice older than 12 months (ages 15, 18, 21, and 21 months) showed mature plasmacytoma histologic features (Table 1), which were not detected in any other organ, indicating the strictly localized nature of the tumor. All of these animals had conspicuous multiorgan lymphoid infiltrates, and 2 of the animals developed amyloidosis involving the kidney and the liver (Figure 5F-G).

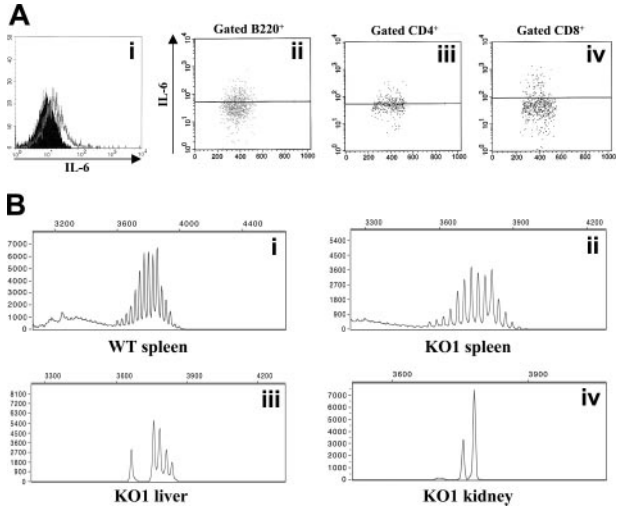

Figure 4. Molecular and immunophenotypic characterization of lymphoid infiltrates in the kidney and the liver. (Ai) Flow cytometric detection of intracellular IL-6 in liver-cell suspension from a 20-month-old *Il12rb2* KO mouse. Open profile is anti–IL-6 mAb staining; dark profile is isotypic control staining. Cells were cultured without stimuli for 16 hours in the presence of brefeldin A to allow intracellular accumulation of synthesized IL-6, permeabilized, and analyzed, gating on lymphocytes according to physical parameters. Staining with anti–IL-6 mAb of liver cells from an age-matched WT mouse yielded completely negative results (not shown). (Aii-iv) Dot-plots showing the results of double staining with anti-B220, CD4 or CD8, and anti–IL-6 mAbs. Gate was set on $B220^+$, $CD4^+$, or $CD8^+$ splenocytes. (B) Ig gene rearrangement studies by Ig CDR3 spectratyping. DNA was extracted from the spleen of a 19-month-old WT (Bi) and an age-matched *Il12rb2* KO mice (Bii), as well from the liver (Biii) and the kidney (Biv) of the latter mouse. PCR amplification was performed by using a set of forward primers designed on an IgV_H chain sequence available on the IMGT database (http://imgt.cines.fr) that detects approximately 55% of IgV_H regions (see "Materials and methods" for further details). Products were run on an automated sequenator and analyzed with Genescan software (Applied Biosystems).

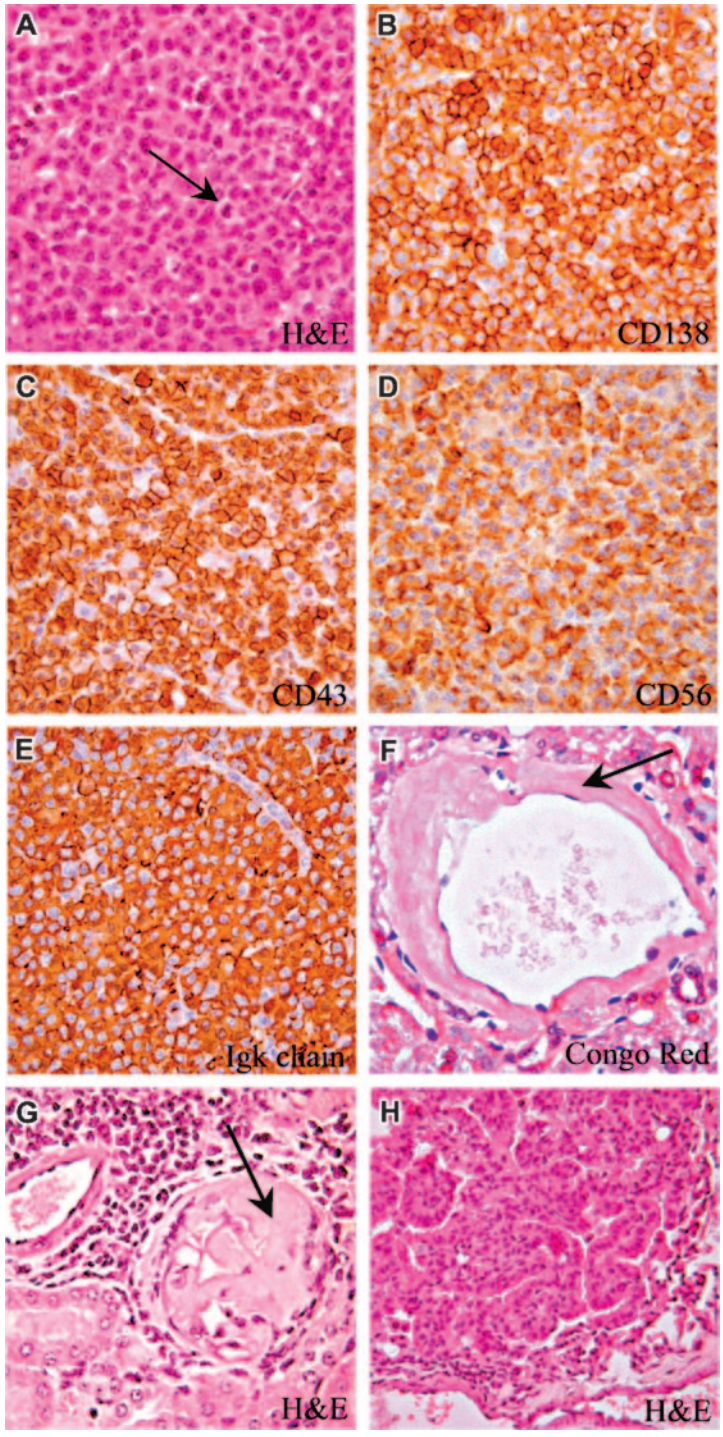

Figure 5. Plasmacytoma and bronchoalveolar carcinoma in *Il12rb2* KO mice. A 21-month-old mouse showing a mature lymph node plasmacytoma with cells characterized by low nuclear-cytoplasmic ratio and abundant cytoplasm (A). Some mitoses are observed (A, arrow). Plasmacytoid cells express CD138 (B), CD43 (C), and CD56 (D). Panels E and F show amyloidosis detected in the liver (F, Congo red staining) and kidney (G, Giemsa staining) from 2 plasmacytoma-bearing mice. A 22-month-old mouse has developed bronchoalveolar carcinoma of the lung. This epithelial tumor is formed of well-differentiated mucin-containing columnar cells lining the respiratory spaces (G). Magnification: (A-G) × 630; (H) × 400.

In the representative case of mature plasmacytoma shown in Figure 5, normal lymph node architecture was completely effaced by plasma cells with eccentric nuclei and low nuclear-cytoplasmic ratio; some mitotic figures were also detected (Figure 5A, arrow). These cells, which replaced the cortex and enlarged the medullary cords, had a $B220^{-}/CD138^{+}/CD56^{+}/CD43^{+}/PCNA^{+/-}$ immunophenotype (Figure 5A-E). Plasma-cell expression of CD56 indicated their malignant nature, since this marker is not detected in normal plasma cells.[19-21] Furthermore, neoplastic plasma cells displayed uniform staining for Ig κ light chains (Figure 5E) in the absence of any reactivity for Igλ, suggesting the monoclonal nature of these proliferations.

Three additional mice (3/10; ie, 30%) aged 3 (not shown), 18, and 22 months (Table 1) developed adenocarcinoma (1 case) or bronchoalveolar lung carcinoma (2 cases) formed by well-differentiated mucin-containing columnar cells that lined respiratory spaces without invading the stroma (Figure 5H). No evidence of epithelial malignancy was observed in other organs.

Reciprocal regulation of IL-6 and IL-12 production in splenocytes from WT mice

In order to investigate the mutual influences of IL-6 and IL-12, adherent cell-depleted splenocytes from WT mice aged 3 to 15

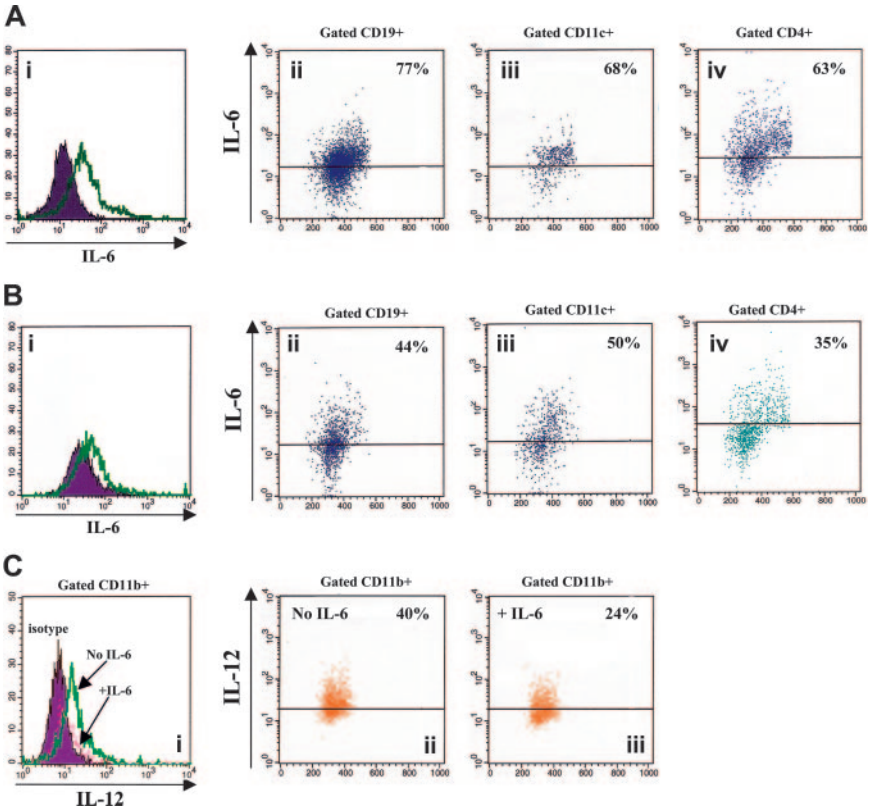

Figure 6. Reciprocal regulation of IL-6 and IL-12 production in splenocytes from WT mice. (Ai,Bi) Flow cytometric detection of intracellular IL-6 in adherent cell-depleted splenocytes cultured with PHA, PMA, LPS, CpG, and calcium ionophore in the absence (A) or presence (B) of murine rIL-12. Open profile is anti–IL-6 mAb staining; dark profile is isotypic control staining. (Aii-iv, Bii-iv) Dot-plots showing the results of double staining with CD19, CD11c, or CD4 and anti–IL-6 mAbs. Gate was set on $CD19^+$, $CD11c^+$, or $CD4^+$ splenocytes, respectively. (C) Flow cytometric detection of intracellular IL-6 in gated $CD11b^+$ macrophages cultured with LPS, CpG, PMA, and calcium ionophore in the presence (+IL-6) or absence (no IL-6) of murine rIL-6. (Ci) Dark profile is isotypic control staining, dashed profile is anti–IL-6 mAb staining in macrophages treated with IL-6, and open profile is anti–IL-6 mAb staining in macrophages cultured without IL-6. (Cii-iii) Dot-plots showing the results of double staining with CD11b and anti–IL-6 mAbs. Gate was set on $CD11b^+$ cells.

months were cultured with various stimuli in the presence or absence of murine rIL-12. IL-6 production by stimulated splenocyte-cell suspensions detected in the absence of rIL-12 (Figure 6Ai) was down-regulated following exposure to the cytokine (Figure 6Bi). In particular, rIL-12 dampened IL-6 production in $CD19^+$ B lymphocytes (76.5% ± 1.33% to 47.5% ± 2.82%, medians ± SE from 6 experiments, Figure 6A-B), $CD11c^+$ myeloid dendritic cells (82% ± 1.36% to 57% ± 3.8%, medians ± SE from 6 experiments, Figure 6A-B), and $CD4^+$ T lymphocytes (59% ± 2.42% to 35% ± 2.13%, medians ± SE from 6 experiments, Figure 6A-B).

Macrophage-enriched adherent splenocytes from WT mice were cultured with various stimuli in the presence or absence of murine rIL-6, and then analyzed for IL-12 production. As shown in Figure 6C, IL-12 production by stimulated $CD11b^+$ macrophages detected in the absence of IL-6 (49.5% ± 2.85%, median ± SE from 4 different experiments) was reduced following treatment with the cytokine (31% ± 2.78%, median ± SE from 4 different experiments).

Discussion

This study demonstrates that *Il12rb2* KO mice developed an autoimmune/lymphoproliferative disorder associated with increased susceptibility to spontaneous tumor formation. These features, which were detected exclusively by histologic analysis, did not reduce significantly the mice's life span.

The autoimmune/lymphoproliferative disorder was characterized by immune-complex–mediated glomerulonephritis, systemic IL-6 up-regulation, and multiorgan lymphoid infiltrates with oligoclonal B-cell expansion. In addition, half of aged *Il12rb2* KO mice developed isolated lymph node plasmacytoma or lung adenocarcinoma or bronchoalveolar carcinoma.

The IL-6 overexpression, which was detected in activated T and B cells from the spleen, the kidney, and the liver of *Il12rb2* KO mice, likely represents a clue to the pathogenesis of the autoimmune/lymphoproliferative disorder here described.

A subset of murine pulmonary dendritic cells was previously shown to produce IL-6 but not IL-12 by default, whereas the same cells switched to IL-12 production in $IL\text{-}6^{-/-}$ mice,[22] indicating that IL-6 dampened IL-12 production. In this study, we demonstrate for the first time a functional antagonism between IL-6 and IL-12, since the former cytokine down-regulated the production of the latter and vice versa in splenocytes from WT mice.

The possibility that part of the pathologic features detected in *Il12rb2* KO mice was related to IL-6 overproduction is supported by previous studies showing that IL-6 transgenic mice developed lymphoproliferation and plasmacytosis culminating, by 18 months of age, in localized lymph node plasmacytoma or in follicular or diffuse large-cell B-cell lymphomas.[23,24] Furthermore, mesangial glomerulonephritis was consistently observed in IL-6 transgenic mice.

Potential mechanisms whereby IL-6 up-regulation may impact on disease development in our model include (1) direct effects on B-cell proliferation and plasma-cell differentiation, (2) block of $CD4^+$, $CD25^+$ regulatory T cells,[25] and (3) induction of Th2 and/or inhibition of Th1 differentiation.[26,27] As for the latter point, the virtual absence of IL-4 and IL-10 in splenocytes from *Il12rb2* KO mice was against "classical" Th2 differentiation. Nonetheless, within the murine T-cell compartment, IL-6 is selectively produced by Th2 cells,[28] and the aberrant B-cell activation detected in *Il12rb2* KO mice is consistent with Th2-like differentiation.

Il12rb2 KO mice followed-up until 3 months of age were found to display impaired IFN-γ production together with defective NK and cytotoxic T-lymphocyte (CTL) activity,[15] which predisposed

these animals to infections with intracellular pathogens.[15] Furthermore, IFN-$\gamma^{-/-}$ C57BL/6 aged mice developed disseminated lymphomas and lung adenocarcinoma.[29] However, these lymphomas were of T-cell lineage,[29] and such tumors were not detected in our *Il12rb2* KO mice, which manifested instead localized plasmacytoma. Immune-complex glomerulonephritis, which was detected in most of our mice, was never reported in IFN-$\gamma^{-/-}$ C57BL/6 mice. Thus, it can be speculated that decreased availability of IFN-γ may be involved in the pathogenesis of lung tumors, but not of other pathologic manifestations detected in *Il12rb2* KO mice.

In conclusion, the present study provides proof of the concept that IL-12 restrains aberrant B-cell activation,[14] since lack of IL-12 signaling resulted in autoimmunity, lymphoproliferation, and increased proneness to tumors derived, in part, from the B-cell lineage.

Thus, *Il12rb2* KO mice may represent a useful model to investigate the relationships between autoimmunity and tumor susceptibility in humans. Studies with human diseases related to the model here described (eg, Sjögren syndrome, localized plasmacytoma, immune-complex glomerulonephritis) will allow the assessment of the potential contribution of mutations or polymorphisms of members of the IL-12/IL-12R gene families to disease development.

Acknowledgments

We are grateful to Dr Peter Isaacson for invaluable help in the interpretation of histologic findings, and Drs Alain Fisher and Antonio Uccelli for helpful discussion, suggestions, and critical revision of the article. We also thank Drs Gian Marco Ghiggeri and Franco Ferrario for helpful discussion. The excellent secretarial assistance of Mrs Chiara Bernardini and the technical support for animal care provided by Mr Giuseppe Taverniti are acknowledged. We thank Drs Vittorio Bocchini and Giovanni Melioli for performing blood and urine chemistry assays, and Dr Anna Favre for the help in the initial histologic studies.

References

1. Trinchieri G. Interleukin-12 and the regulation of innate resistance and adaptive immunity. Nat Rev Immunol. 2003;3:133-146.
2. Stern AS, Podlaski FJ, Hulmes JD, et al. Purification to homogeneity and partial characterization of cytotoxic lymphocyte maturation factor from human B-lymphoblastoid cells. Proc Natl Acad Sci U S A. 1990;87:6808-6812.
3. Wolf SF, Temple PA, Kobayashi M, et al. Cloning of cDNA for natural killer cell stimulatory factor, a heterodimeric cytokine with multiple biologic effects on T and natural killer cells. J Immunol. 1991;146:3074-3081.
4. Manetti R, Gerosa F, Giudizi MG, et al. Interleukin 12 induces stable priming for interferon gamma (IFN-gamma) production during differentiation of human T helper (Th) cells and transient IFN-gamma production in established Th2 cell clones. J Exp Med. 1994;179:1273-1283.
5. Magram J, Sfarra J, Connaughton S, et al. IL-12-deficient mice are defective but not devoid of type 1 cytokine responses. Ann N Y Acad Sci. 1996; 795:60-70.
6. Smyth MJ, Taniguchi M, Street SE. The anti-tumor activity of IL-12: mechanisms of innate immunity that are model and dose dependent. J Immunol. 2000;165:2665-2670.
7. Brunda MJ, Luistro L, Warrier RR, et al. Antitumor and antimetastatic activity of interleukin 12 against murine tumors. J Exp Med. 1993;178:1223-1230.
8. Colombo MP, Trinchieri G. Interleukin-12 in anti-tumor immunity and immunotherapy. Cytokine Growth Factor Rev. 2002;13:155-168.
9. Nanni P, Nicoletti G, De Giovanni C, et al. Combined allogeneic tumor cell vaccination and systemic interleukin 12 prevents mammary carcinogenesis in HER-2/neu transgenic mice. J Exp Med. 2001;194:1195-1205.
10. Presky DH, Yang H, Minetti LJ, et al. A functional interleukin 12 receptor complex is composed of two beta-type cytokine receptor subunits. Proc Natl Acad Sci U S A. 1996;93:14002-14007.
11. Chua AO, Chizzonite R, Desai BB, et al. Expression cloning of a human IL-12 receptor component: a new member of the cytokine receptor superfamily with strong homology to gp130. J Immunol. 1994;153:128-136.
12. Trinchieri G, Pflanz S, Kastelein RA. The IL-12 family of heterodimeric cytokines: new players in the regulation of T cell responses. Immunity. 2003;19:641-644.
13. Airoldi I, Gri G, Marshall JD, et al. Expression and function of IL-12 and IL-18 receptors on human tonsillar B cells. J Immunol. 2000;165:6880-6888.
14. Airoldi I, Di Carlo E, Banelli B, et al. The IL-12Rbeta2 gene functions as a tumor suppressor in human B cell malignancies. J Clin Invest. 2004; 113:1651-1659.
15. Wu C, Wang X, Gadina M, O'Shea JJ, Presky DH, Magram J. IL-12 receptor beta 2 (IL-12R beta 2)-deficient mice are defective in IL-12-mediated signaling despite the presence of high affinity IL-12 binding sites. J Immunol. 2000;165:6221-6228.
16. Airoldi I, Guglielmino R, Carra G, et al. The interleukin-12 and interleukin-12 receptor system in normal and transformed human B lymphocytes. Haematologica. 2002;87:434-442.
17. Brignole C, Pastorino F, Marimpietri D, et al. Immune cell-mediated antitumor activities of GD2-targeted liposomal c-myb antisense oligonucleotides containing CpG motifs. J Natl Cancer Inst. 2004;96:1171-1180.
18. Wiken M, Bjorck P, Axelsson B, Perlmann P. Studies on the role of CD43 in human B-cell activation and differentiation. Scand J Immunol. 1989;29:353-361.
19. Harada H, Kawano MM, Huang N, et al. Phenotypic difference of normal plasma cells from mature myeloma cells. Blood. 1993;81:2658-2663.
20. Kaiser U, Auerbach B, Oldenburg M. The neural cell adhesion molecule NCAM in multiple myeloma. Leuk Lymphoma. 1996;20:389-395.
21. Martin P, Santon A, Bellas C. Neural cell adhesion molecule expression in plasma cells in bone marrow biopsies and aspirates allows discrimination between multiple myeloma, monoclonal gammopathy of uncertain significance and polyclonal plasmacytosis. Histopathology. 2004;44:375-380.
22. Dodge IL, Carr MW, Cernadas M, Brenner MB. IL-6 production by pulmonary dendritic cells impedes Th1 immune responses. J Immunol. 2003; 170:4457-4464.
23. Kovalchuk AL, Kim JS, Park SS, et al. IL-6 transgenic mouse model for extraosseous plasmacytoma. Proc Natl Acad Sci U S A. 2002;99:1509-1514.
24. Ishihara K, Hirano T. IL-6 in autoimmune disease and chronic inflammatory proliferative disease. Cytokine Growth Factor Rev. 2002;13:357-368.
25. Pasare C, Medzhitov R. Toll pathway-dependent blockade of CD4+CD25+ T cell-mediated suppression by dendritic cells. Science. 2003;299: 1033-1036.
26. Rincon M, Anguita J, Nakamura T, Fikrig E, Flavell RA. Interleukin (IL)-6 directs the differentiation of IL-4-producing CD4+ T cells. J Exp Med. 1997;185:461-469.
27. Diehl S, Anguita J, Hoffmeyer A, et al. Inhibition of Th1 differentiation by IL-6 is mediated by SOCS1. Immunity. 2000;13:805-815.
28. Zubiaga AM, Munoz E, Merrow M, Huber BT. Regulation of interleukin 6 production in T helper cells. Int Immunol. 1990;2:1047-1054.
29. Street SE, Trapani JA, MacGregor D, Smyth MJ. Suppression of lymphoma and epithelial malignancies effected by interferon gamma. J Exp Med. 2002;196:129-134.
30. Le Franc M-P. IMGT, ImMunoGeneTics information system. http://imgt.cines.fr. Accessed April 10-15, 2005.